Observation of Rayleigh-Taylor-like Structures in a Laser-Accelerated Foil

R. R. Whitlock, M. H. Emery, J. A. Stamper, E. A. McLean, S. P. Obenschain, and M. C. Peckerar
Naval Research Laboratory, Washington, D.C. 20375
(Received 28 September 1983)

The development of the Rayleigh-Taylor hydrodynamic instability was studied in laser-accelerated targets by introduction of mass thickness variations in foil targets. Observations made by side-on flash x radiography showed target structures and mass redistribution effects which resemble Rayleigh-Taylor bubbles and spikes, including not only advanced broadening of the spike tips on the laser-irradiated side of the foil but also projections of mass on the unirradiated side. The observations compare well with numerical simulations.

PACS numbers: 52.50.Jm, 52.35.Py, 52.65+z

The Rayleigh-Taylor[1] (RT) hydrodynamic instability can arise when a fluid of lower density accelerates a fluid layer of a higher density. The RT instability causes ripples at the interface between the fluids to grow in amplitude until the fluids interpenetrate each other as bubbles (of the lower-density fluid) and spikes (of the higher-density fluid), which can eventually shred the interface. The spikes grow as dense protrusions into the lighter material, locally increasing the mass thickness normal to the original interface. In the nonlinear regime, the spike tips can develop a mushroom shape similar to a Kelvin-Helmholtz[2] rollup.[3] In addition, the confluence of mass into the spike can result in protrusions on the rear of the denser layer.[4] Using x radiography, we have obtained the first images of a laser-accelerated foil showing structures which resemble these Rayleigh-Taylor signatures. Such phenomena are of concern to inertial confinement fusion,[3-5] since implosion symmetry and fuel integrity may be spoiled by the RT instability.

Previous experiments with laser-accelerated targets without intentional target nonuniformities yielded no observable RT growth.[6] The first use of rippled and bar targets showed growth of initial perturbations, although the mechanisms remained in question.[7] Measured growth rates of mass modulations developing in corrugated foils, examined by streaked x radiography viewing normal to the foil, were in agreement with RT numerical simulations.[8] A face-on flash-x-radiographic technique[9] using bar targets has recently shown evidence for RT growth.

In this work, planar foils were structured periodically in mass thickness, in order to initiate the hydrodynamic instabilities with a predetermined wavelength. The spatial wavelength λ and thickness of the mass modulations were varied. The targets were made of plastic (1.0 g/cm^3), having rectangular bars of length L, of width $\lambda/2$ and separated by $\lambda/2$, placed on the rear (nonirradiated) side of a base foil (see Fig. 1). The foils were irradiated at 5×10^{12} W/cm^2 [computed from the temporal full width at half maximum (FWHM) and the 90% energy contour of an equivalent focus] in the quasi-near field of a single driver beam of the Pharos II Nd-glass laser operating at 1.05-μm wavelength with a 4-ns pulse. The focal diameter was 650 μm. The bar length L for backlighting was 400 μm, i.e., less than the focal diameter. The laser's second beam was shortened to $\sim$300 ps and directed onto an adjacent Al target at 45° incidence to produce a flash backlighting source of 1.6-keV x rays[10] delayed $\sim$6 ns after the peak of the driver pulse. A pinhole array imaged the x-ray source and also

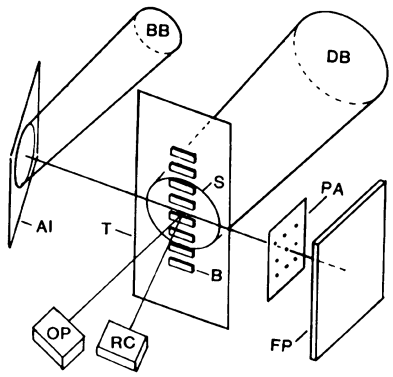

FIG. 1. Setup. Driver laser beam (DB) was focused into a large spot (S) at 6° incidence onto a plastic foil target (T) having bars (B) on the rear. An optical pyrometer (OP) and an x-ray pinhole camera (RC) viewed from the rear. A second laser beam (BB) irradiated an Al target (Al) to provide a backlighting x-ray flash for radiography of the accelerated foil using a pinhole array (PA) to image onto a film pack (FP).

Work of the U. S. Government
Not subject to U. S. copyright

viewed parallel to the bars on the foil to produce x radiographs at a magnification of 3.0; resolution was 10 μm, i.e., measurements are $\sim \pm 5\mu$m. Another pinhole camera, behind and 20° from the target normal, recorded the self-emission of the accelerated foil and verified alignment of the bars.

Pyrometric blackbody-brightness measurements[11] of the rear of the targets gave temperatures of only 4.5 ± 1 eV, regardless of target structure (unperturbed or $\lambda = 8$, 25, or 50 μm) on nonbacklighting shots, as well as on two backlighting shots. Thus, the backlighter did not appreciably heat the driven foil. Rear pinhole images and laser-focal diagnostics showed circular fringes in the incident beam and also a pattern of 40–50-μm bands parallel to the bars in perturbed targets. The effects of this laser nonuniformity are observable in the original radiograph of an accelerated unperturbed target as a gentle modulation in the accelerated target [Fig. 2(b)].

Perturbed targets were accelerated under the same illumination conditions. For these targets, the base thickness was 9.7 μm, i.e., about five ablation depths.[12] The bar thickness was systematically increased to 2.7 μm, but all had $\lambda = 50$ μm. A modulation of 50-μm periodicity is observed in the radiograph of an accelerated foil with 0.5-μm-thick bars [Fig. 2(c)], for an impressed thickness ratio of $1.05 = (9.7 + 0.5)/9.7$. Darker regions correspond to higher x-ray absorption and higher areal mass density. For an increased thickness ratio of 1.15 the striations of higher and lower density regions are more accentuated [Fig. 2(d)]. The mean target displacement was about 140 μm, with dense material extending rearward as far as 200 μm. Larger displacements (accelerations) off the axis of the focus result from an annular region of increased incident irradiance.

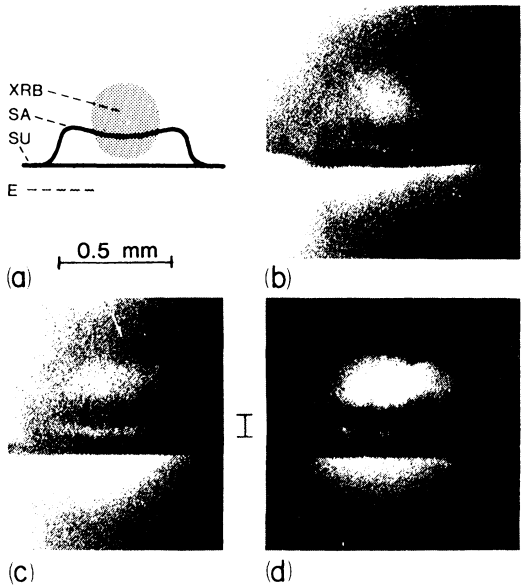

FIG. 2. (a) Schematic of radiographs, laser incident from below, including *E*, self-emission from blowoff of driven foil; SU, shadow of unaccelerated margin of foil; XRB, region of x-ray backlighting; and SA, shadow of accelerated foil (only part of which is seen in any one radiograph), and distance scale for (b)–(d). Light regions in left corners of radiographs are from nearby pinholes. (b) Radiograph of an 11.2-μm unperturbed target. (c) Radiograph of bar target with 1.05 thickness ratio. Between (c) and (d) is a 140-μm marker. (d) Bar target with 1.15 initial thickness ratio.

In a radiograph of this annular region at the still greater thickness ratio of 1.3, the tips of the denser structures become pronounced and are seen to extend from the accelerated region of the foil proper back toward the laser. In Fig. 3, we compare the experimental radiograph [Fig. 3(a)] with numerical simulation results. Note especially the identifications of the spike and bubble regions. The projection of dense mass protrusions back toward the laser (downward in Fig. 3) is characteristic of spikes in the Rayleigh-Taylor instability. In Fig. 3(a), a bridge, at least 3 times thinner than the 80 ± 5 μm axial extent of the accelerated unperturbed target, appears to connect neighboring spikes. The spikes extend about 60 ± 5 μm to the front (toward the laser) of this bridge. Smaller projections of mass are also observed to the rear of each spike. Photometric measurements of x-ray intensities[10] in the images of the spike tips and the intervening bubble regions were made with calibrated photographic emulsion.[13] Self-emission of the foil was negligible. Converting these measurements to average mass thicknesses as in Ref. 10 yields densities at least 0.10 of solid in the spikes, if we assume an x-ray path length equal to the bar length. Bubble densities are smaller than spike densities by factors of 2.5–4. Accounting for the presence in the x-ray path of the target material at the rim of the focal spot would increase this factor. The overall axial extent, from tip to rear of the target shadow, is about 105 μm, which is greater than the unperturbed target (80 ± 5 μm). These modulations in mass density, and the thinness of the bridge region, indicate that mass redistribution has taken place leaving bubble volumes deficient in mass. The projected radiographic image of the spike tips also appears to exhibit advanced lateral broadening, indicative of the nonlinear stage of the RT instability.[14,15]

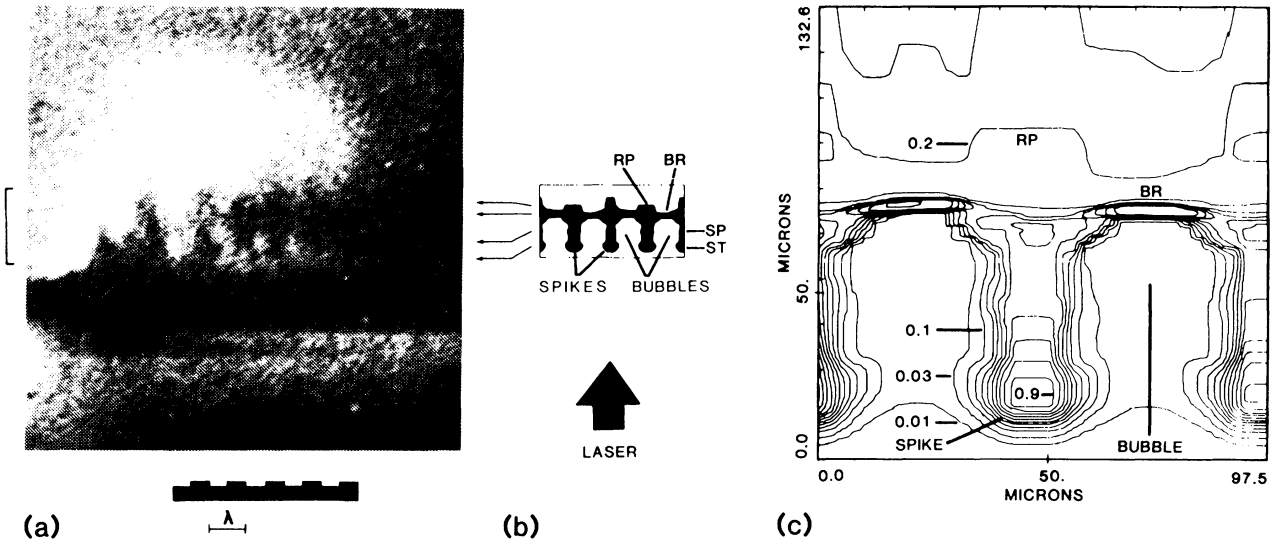

FIG. 3. Comparison of results for thickness ratio of 1.3 and $\lambda = 50$ μm. Laser incident from below, target acceleration upward, direction of spike growth downward. (a) Experimental radiograph of bar target. Initial cross section and scale ($\lambda = 50$ μm, thickness exaggerated) is diagrammed below image. Within the backlit region (upper $\frac{2}{3}$ of image), dense target material (including spikes, rear projections, and bridge) appears dark; low-density regions (bubbles, area to rear of accelerated target) appear bright. Accelerated target is to right of bracket. (b) Numerical simulation of accelerated target. The $0.2\rho_{max}$ contour from (c) is repeated to show multiple spikes and demagnified so that the lateral scale of (b) matches (a). Axial positions of corresponding features are conveyed by horizontal arrows extending from (b) to (a). Features of major importance are identified as spikes, bubbles, ST (spike tip), SP (spike), BR (bridge), and RP (rear projection). (c) Isodensity contours from FAST2D simulation at τ_{delay} for conditions given in text. Contours are in 0.10 increments of the maximum ($\rho_{max} = 0.661$ g/cm^3), with additional contours at 0.03 and 0.01 of ρ_{max}. Bubbles are the large, mass-deficient volumes (between the 0.01 and 0.03 contours). Development of spike, bubble, and rear projections, as well as broadening of the spike tips, is evident in these experimental and numerical results.

These highly developed features are compared below with numerical simulation.

The evolution of a perturbed target under conditions similar to those of the experiment was modeled with the FAST2D[3,14] laser-shell simulation code. For the numerical run shown in Fig. 3(c), the initial target mass was structured the same as the experimental target of Fig. 3(a), while the incident laser intensity was 8×10^{12} W/cm^2 in a $\tau_{laser} = 5$ ns FWHM pulse. The average final target velocity was 3.8×10^6 cm/s and the total distance pushed (measured in the bridge connecting the spikes at $\tau_{delay} = 5$ ns) was 180 μm. Rear surface temperatures were 4–6 eV at τ_{delay}. The most unstable mode, $\lambda = 50$ μm $= 2\pi/k$, follows an initial phase of amplitude decay while the flow patterns evolve into an eigenmode and then grows exponentially by mass redistribution until $kA \approx 1$, after which the amplitude A of the perturbation grows at the slower free-fall rate,[14] $\Delta A = \frac{1}{2}g(\Delta t)^2$, with $g = 1.56$ μm/ns^2.

The exponential growth rate was measured numerically to be 7×10^8 s^{-1}, which is about 1.5 times smaller than the linear classical value, in good agreement with the linear growth rates of long-wavelength sinusoidal perturbations for constant laser intensity.[14] There were 3 e-foldings of exponential growth above the minimum amplitude. The spike-bubble amplitude (on the 30% density contour) at τ_{delay} is 65 μm [Fig. 3(c)], which compares favorably with experimental observation (60 ± 5 μm).

An experimental growth factor of $22 = (60$ μm$)/(2.7$ μm$)$, over a growth time of no more than $\tau_{delay} + \tau_{laser}$, implies an exponential growth rate greater than $\gamma_{min} = \ln(22)/10$ ns $= 3\times10^8$ s^{-1}. Accounting for initial or free-fall phases of evolution would give larger growth rates. The final amplitude may be compared to a simple model in which exponential growth proceeds at the linear classical rate, and in which the initial phase, the free-fall rate, and the amplitude of transition to free fall are as simulated numerically; the calculated final amplitude is greater than that observed by a factor of 1.5.

The nonlinear Kelvin-Helmholtz-like spike-tip broadening[14,15] is clearly evident in Fig. 3(c). The vorticity generated by the noncollinear nature of the density and pressure profiles collects behind the heads of the spikes causing the spike tips to widen. This effect becomes appreciable when the amplitude of the perturbation is about half the wavelength of the perturbation.[14] The 20% density contour at the rear of the target, Figs. 3(b) and 3(c), delineates rearward mass projections similar to those found experimentally. These projections in the simulation are due to the collision of mass flowing from adjacent bubble regions into an intermediate spike, resulting not only in spike growth but also in a rearward jetting.[4]

Several mechanisms other than RT were considered: differences in acceleration for thicker and thinner portions of bar targets; preferential thermal broadening of the spike tips; various geometric mechanisms such as viewing parallax; etc. From the combination of the observed structures and simulation results on temperature contours, the most likely explanation for the structures in the radiographs remains hydrodynamic instability.

In summary, several basic features of the advanced development of the RT hydrodynamic instability have been identified in the numerical results and compared with experimental observations. The observations are consistent with mass redistribution into a high-density spike and a mass-deficient bubble, with broadening of the spike tips. Moreover, rearward projections were observed experimentally and interpreted with the numerical simulation results. Mass redistribution processes such as those observed could significantly affect inertial-fusion pellet performance. Extensive further experimental work is needed to relate these hydrodynamic phenomena to laser-fusion reactor scenarios.

The authors acknowledge helpful discussions with B. H. Ripin, S. E. Bodner, D. B. Brown, J. H. Gardner, J. Grun, and D. J. Nagel. We are further appreciative of the expert technical efforts of J. Bass, D. Cheville, W. Griffith, K. R. Hudson, K. Kearney, W. Naffey, D. Newman, N. Nocerino, M. Rebbert, and E. Turbyfill. This research was supported by the U.S. Department of Energy.

[1]Lord Rayleigh, *Theory of Sound* (Dover, New York, 1945), 2nd ed., Vol. 2; G. I. Taylor, Proc. Roy. Soc. London, Ser. A 210, 192 (1950).

[2]H. Helmholtz, Philos. Mag., Ser. 4 36, 337 (1868); Lord Kelvin, *Hydrodynamics and General Dynamics* (Cambridge Univ. Press, Cambridge, England, 1910), pp. 69ff.

[3]M. H. Emery *et al.*, Phys. Rev. Lett. 48, 667 (1982).

[4]E. Ott, Phys. Rev. Lett. 29, 1429 (1972); C. P. Verdon *et al.*, Phys. Fluids 25, 1653 (1982).

[5]J. N. Shiau *et al.*, Phys. Rev. Lett. 32, 352 (1974); J. D. Lindl and W. C. Mead, Phys. Rev. Lett. 34, 1273 (1975); G. Fraley *et al.*, in *Plasma Physics and Controlled Nuclear Fusion Research—1974*, IAEA-CN-33 F-5-5 (International Atomic Energy Agency, Vienna, 1975); R. G. Evans *et al.*, Phys. Rev. Lett. 49, 1639 (1982).

[6]A. Raven *et al.*, Phys. Rev. Lett. 47, 1049 (1981); J. D. Kilkenny *et al.*, J. Phys. D 13, L123 (1980).

[7]B. H. Ripin *et al.*, Bull. Am. Phys. Soc. 25, 946 (1980).

[8]A. J. Cole *et al.*, Nature (London) 299, 329 (1982).

[9]J. Grun *et al.*, Naval Research Laboratory Report No. NRL-MR 4896, 1983 (unpublished).

[10]R. R. Whitlock *et al.*, Appl. Phys. Lett. 41, 429 (1982).

[11]E. A. McLean *et al.*, Phys. Rev. Lett. 45, 1246 (1980).

[12]J. Grun *et al.*, Appl. Phys. Lett. 39, 545 (1981).

[13]R. F. Benjamin *et al.*, Appl. Opt. 16, 393 (1977).

[14]M. H. Emery *et al.*, Appl. Phys. Lett. 41, 808 (1982), and erratum (to be published).

[15]B. J. Daly, Phys. Fluids 10, 297 (1967).

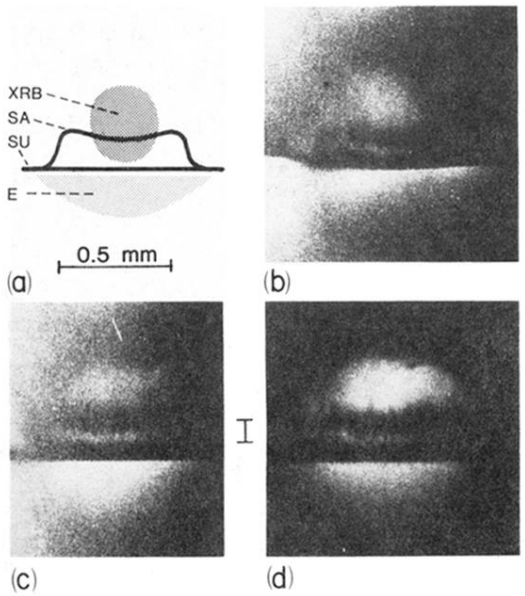

FIG. 2. (a) Schematic of radiographs, laser incident from below, including *E*, self-emission from blowoff of driven foil; SU, shadow of unaccelerated margin of foil; XRB, region of x-ray backlighting; and SA, shadow of accelerated foil (only part of which is seen in any one radiograph), and distance scale for (b)–(d). Light regions in left corners of radiographs are from nearby pinholes. (b) Radiograph of an 11.2-μm unperturbed target. (c) Radiograph of bar target with 1.05 thickness ratio. Between (c) and (d) is a 140-μm marker. (d) Bar target with 1.15 initial thickness ratio.

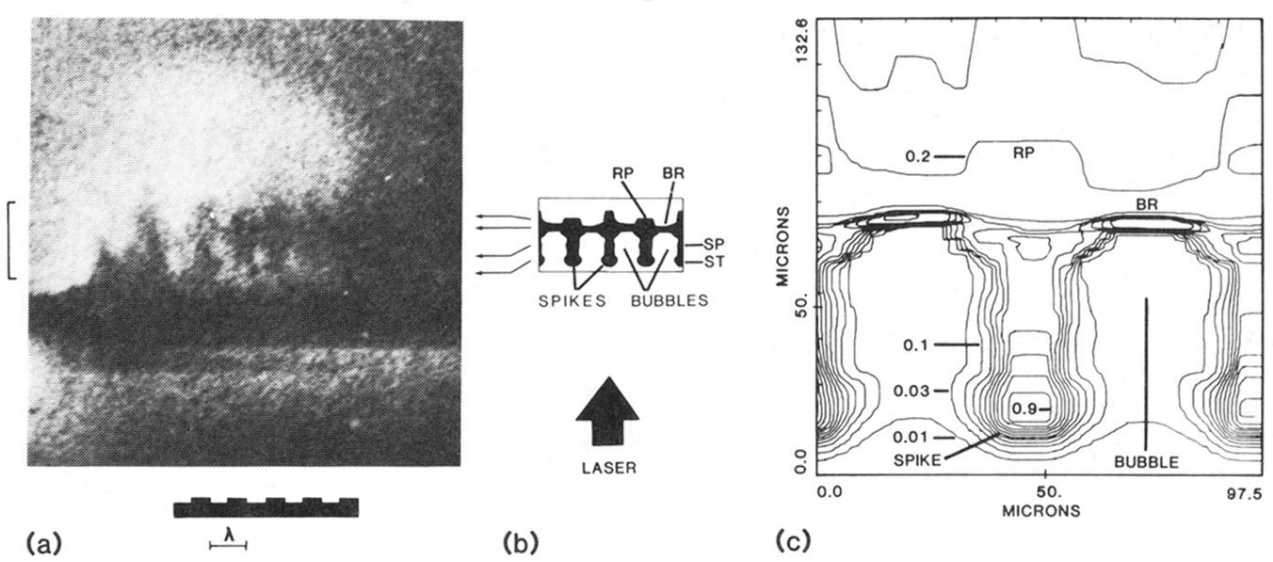

FIG. 3. Comparison of results for thickness ratio of 1.3 and $\lambda = 50$ μm. Laser incident from below, target acceleration upward, direction of spike growth downward. (a) Experimental radiograph of bar target. Initial cross section and scale ($\lambda = 50$ μm, thickness exaggerated) is diagrammed below image. Within the backlit region (upper $\frac{2}{3}$ of image), dense target material (including spikes, rear projections, and bridge) appears dark; low-density regions (bubbles, area to rear of accelerated target) appear bright. Accelerated target is to right of bracket. (b) Numerical simulation of accelerated target. The $0.2\rho_{max}$ contour from (c) is repeated to show multiple spikes and demagnified so that the lateral scale of (b) matches (a). Axial positions of corresponding features are conveyed by horizontal arrows extending from (b) to (a). Features of major importance are identified as spikes, bubbles, ST (spike tip), SP (spike), BR (bridge), and RP (rear projection). (c) Isodensity contours from FAST2D simulation at τ_{delay} for conditions given in text. Contours are in 0.10 increments of the maximum ($\rho_{max} = 0.661$ g/cm^3), with additional contours at 0.03 and 0.01 of ρ_{max}. Bubbles are the large, mass-deficient volumes (between the 0.01 and 0.03 contours). Development of spike, bubble, and rear projections, as well as broadening of the spike tips, is evident in these experimental and numerical results.